Article:
Wang, Q, Shen, J, Glover, PWJ et al. (2022) Oil production enhancement, asphaltene precipitation and permeability damage during CO2-SAG flooding of multi-layer sandstone reservoirs. Journal of Petroleum Science and Engineering, 212. 110241. ISSN: 0920-4105

https://doi.org/10.1016/j.petrol.2022.110241

Oil production enhancement, asphaltene precipitation and permeability damage during CO_2-SAG flooding of multi-layer sandstone reservoirs

Qian Wang[1*], Jian Shen[1], Paul W.J. Glover[2], Piroska Lorinczi[2], Wei Zhao[3]

[1]School of Resources and Geosciences, China University of Mining and Technology, Xuzhou, 221116, China

[2]School of Earth and Environment, University of Leeds, Leeds, LS2 9JT, UK

[3]China Petroleum Technology and Development Corporation, Beijing, 100028, China

Abstract: The process of CO_2-SAG flooding involves conventional miscible CO_2 flooding until breakthrough (BT), followed by a period of CO_2 soaking or shut-in, and then a continuation of the miscible CO_2 flooding. The SAG process provides different improvement in the oil recovery for different positions of each layer in multilayer reservoirs, and has different effects on the distribution of pore throat blocking and adsorption of asphaltene to mineral surfaces. In this paper, both miscible CO_2-SAG and conventional CO_2 flooding experiments have been carried out at reservoir conditions and on multi-layer systems composed of parallel connection of long cores. After CO_2-SAG flooding oil recovery factors (RF) of the low, medium and high permeability cores were 7.7%, 8.3%, and 7.6% higher compared to the RFs after CO_2 flooding. The respective fractional oil production (FOP) of each long core were 10.6%, 27.7%, and 61.6% after CO_2-SAG flooding, with less difference between each long core than CO_2 flooding. After CO_2 flooding, the permeability of the high permeability core at the injection end dropped by 24.5-25.8%, which is 5.5-14.3% higher than the value at the outlet. The permeability decrease due to CO_2-SAG flooding was 0.7-9.7% higher than that due to CO_2 flooding, and the distribution of permeability decline is more homogeneous. The contribution of the total permeability decrease attributable to asphaltene particle blockage due to CO_2 flooding was 84.7-62.7%, 5.2-10.1% higher than that due to CO_2-SAG flooding, gradually decreasing along the flow direction. Complex two phase flow of oil and gas is more likely to cause pore throat blockage instead of causing the adsorption of asphaltene precipitation.

Keywords: CO_2-SAG flooding, multilayer reservoirs, asphaltene precipitation, blockage and absorption, permeability decline.

Introduction

The injection of CO_2 into reservoirs is a proven effective enhanced oil recovery (EOR) method[1-3]. Oil viscosity and interfacial tension reduction, volume swelling, light-hydrocarbon extraction during CO_2 flooding are all important effects which contribute to the EOR process[4-5]. Continuous miscible CO_2 flooding is a practical and efficient displacement technology[6]. Regrettably, conventional CO_2 injection suffers from flow instability and viscous fingering, and consequently, early CO_2 breakthrough[7]. Especially, most oil reservoirs are composed of a series of relatively layers with variable permeabilities. In these reservoirs, CO_2 breakthrough occurs first from layers of high permeability. The gas pathway is established through these high permeability layers, which results in a large volume of crude oil in lower permeability layers being by-passed and, consequently, unproduced [8-9].

The CO_2-soaking-alternating-gas flooding process (CO_2-SAG) is a combination of conventional continuous miscible CO_2 flooding with a CO_2 soaking stage from the CO_2 huff-and-puff process[10]. In the first stage CO_2 is continuously injected into the reservoir in the same way as in the conventional miscible CO_2 process. The CO_2-SAG process differs from conventional CO_2 flooding by being stopped at breakthrough. The second stage of the CO_2-SAG process is a soaking period, in which both the injector and producer are shut in. During this period the injected CO_2 diffuses into the residual oil and water in the reservoir, accessing those fluids with which the gas was not in contact during the dynamic first stage of the process. The oil becomes larger in volume and significantly more mobile, allowing it to leave some of the smaller and more inaccessible pores and occupy instead the CO_2 saturated high permeability

channels opened up by the initial flooding in Stage 1 to CO_2 BT [11].The third stage is another simple miscible CO_2 flood to displace and recover the residual oil that was freed in Stage 2[12].

The CO_2-SAG process results in better dissolution of CO_2 in crude oil than either the CO_2 huff-and-puff process, which depends only on the diffusion of molecular CO_2, or conventional CO_2 flooding, where CO_2 only dissolves in the crude oil in direct dynamical contact with the flood front. The improved interaction between CO_2 and crude oil that occurs during the soaking process substantially promotes the miscibility of oil and CO_2, and increases the CO_2 displacement efficiency during secondary CO_2 flooding, with higher CO_2 utilization efficiency and lower injection cost [13].

No matter what kind of CO_2 flooding method is adopted, the CO_2 dissolution or light component stripping of crude oil perturbs crude oil thermodynamically, which promotes the precipitation and flocculation of asphaltenes [14-15]. A proportion of these particles of asphaltene become adsorbed onto mineral surfaces within the rock matrix altering the wettability and hence capillary properties and permeability of the rock. The remaining asphaltene agglomerates remain suspended in the fluid and are transported by the pore fluids until they become trapped in pores and pre throats leading to blockages. These blockages can result in extremely significant drops of permeability[16-17].

Moreover, heterogeneity has a markedly important influence on the final efficacy of the CO_2-SAG process[20]. In multilayer reservoirs the enhancement depends on the quality of the reservoir rock in a given layer and its position along the core as well as the proximity of other layers with different flow characteristics. Reservoir heterogeneity between layers with different permeability also affects the distribution and amount of reservoir damage after flooding[18-20]. In addition, the adsorption and blockage of asphaltene precipitation cause different damage to the permeability at different locations within the reservoir, with different adsorption and blockage mechanisms[21].

In order to formulate more targeted and effective measures in heterogeneous layered reservoir, as well as to prevent or reduce the damage to rock permeability caused by asphaltene precipitation, distinguishing the damage to permeability from blockage and adsorption is required. As a result, the quantification of the influence of the CO_2-SAG process on oil recovery must also be balanced by any deleterious effect on permeability.

There is a relatively small number of core-flooding experiments which have focused on the technical potential of CO_2-SAG flooding. Nevertheless, they permit a number of key issues to be targeted for further study, such as CO_2 injection flow rate and pressure, the parameters which control the optimal CO_2 soaking period, the effect of water pre-flooding, cores with different permeability were subjected to CO_2-SAG flooding experiments under different conditions [12,22]. We have carried out SAG flooding experiments on cores with similar permeability but different pore throat structures and single heterogeneous long cores, and studied the effects of pore structure and linear heterogeneity on the micro and macro crude oil production improvement of CO_2-SAG flooding and the distribution of permeability damage[10,13]. Furthermore, there has been no previous study of the combined improvement in hydrocarbon recovery and progress of permeability damage in heterogeneous reservoirs consisting of multiple layers of rocks with different pore microstructures after both types of flooding. In particular, there is a lack of research on the distribution of asphaltene precipitation in the blocked and adsorbed state.

In this paper, CO_2-SAG and conventional CO_2 flooding have been carried out at reservoir conditions on two assemblages of three long cores with different permeability ,which are arranged in parallel in separate core holders and representing three parallel layers in a reservoir. The porosity and permeability between the analogue cores in the two assemblages are almost the same. The results presented in this paper cover the comparison of the efficiency of miscible CO_2-SAG flooding with simple miscible CO_2 flooding, focusing on (i) fluid displacement, (ii) oil production enhancement and its distribution, (iii) the distribution of permeability damage due to the blockage and adsorption of asphaltene precipitation. The

progress and extent of each effect has been compared across each of the three different pore microstructures (layers). The results furnish information allowing the advantages, disadvantages, benefits and risks of different CO_2 flooding methodologies to be judged in heterogeneous layered reservoir, especially with regard to reservoir damage and the saturation of residual oil.

Methodology

Materials

A crude oil sample taken from the Jilin oilfield in the northeast of China and analyzed to obtain its composition(table 1). The compositional results were used to synthesize a live oil, which was subsequently used in all of the experiments. The proportion of *n*-C_5-insoluble asphaltene in the Jilin oil sample was 3.18 wt% [10]. The minimum miscible pressure of the CO_2-crude oil system was measured by slim-tube apparatus and discovered to be 20.6±0.4 MPa at 90±0.1°C[10]. The relationship between asphaltene precipitation and the crude oil CO_2 concentration has also been measured previously[10], asphaltenes begin to precipitate from crude oil at a dissolved CO_2 concentration of 29.5mol%, and completely precipitate at 60 mol%. as well as being predicted using the Flory-Huggins model[15]. We note that the measured and predicted values differ by <5%. The CO_2 solubility in the Jilin crude oil is 68.3 mol% and the oil viscosity decreases from 2.11 mPa·s (0 mol% CO_2) to 0.62 mPa·s (68.3 mol% CO_2) at 23 MPa and 90°C [10].

This study used two types of brine. The first was prepared to the compositional recipe given in Table 2[10]. The second was prepared from the same compositional recipe but with the addition of Mn^{2+}, which was added to remove the signal arising from water when making nuclear magnetic resonance (NMR) measurements in order to obtain the oil distribution in the core[23].

Table 1. Basic physical properties of live oil together with its compositional analysis (n-C5 insoluble asphaltene content =3.18 wt%).

Property			**Value**		
Density (g/cm^3)			0.731±0.002 (90°C)		
Viscosity (mPa·s)			2.11±0.04 (90°C)		
Solution gas-oil ratio (m^3/m^3)			44.7		
Bubble point pressure (MPa)			6.95		
Composition					
Carbon number	**wt%**	**Carbon number**	**wt%**	**Carbon number**	**wt%**
CO_2	0.053	C9	4.640	C21	2.16
N2	0.422	C10	4.531	C22	2.304
C1	1.741	C11	3.947	C23	2.104
C2	1.126	C12	3.615	C24	2.088
C3	0.998	C13	3.261	C25	1.948
iC4	0.178	C14	2.908	C26	1.872
nC4	0.525	C15	2.633	C27	1.896
iC5	0.942	C16	3.615	C28	1.766
nC5	0.353	C17	3.567	C29	1.882
C6	1.365	C18	3.222	C30+	26.363
C7	2.52	C19	2.484	**Total**	**100**
C8	4.409	C20	2.563		

Table 2. Physicochemical properties of the reservoir brine.

Item	**Value**
Density (g/cm^3)	1.005
Viscosity at 25°C (mPa·s)	1.02
pH	7.04
K^+ (mg/L)	1473
Na^+ (mg/L)	3546
Ca^{2+} (mg/L)	116

Mg^{2+} (mg/L)	33
Cl^- (mg/L)	5261
SO_4^{2-} (mg/L)	1288
HCO_3^- (mg/L)	1559
TDS (mg/L)	13276

142 TDS = Total dissolved solids.

143

144 The artificial long cores used in the tests are composed of epoxy resin and quartz sand with
145 different grain size distributions, which were cold isostatically pressed[24] (Figure 1). The
146 petrophysical characteristics of these core samples are shown in Table 3. The long cores are
147 approximately homogeneous (the difference between the porosity or permeability at any
148 position in the sample is within ±2.7% and ±3.3% of the mean porosity or permeability value
149 for the core, respectively). Three cores with different permeabilities and porosities were used
150 in a triad to represent three reservoir layers with different permeabilities. Consequently, though
151 the results discussed in this paper refer to three different cores, they represent analogue layers
152 in a reservoir.

153

154
155 **Figure 1.** Schematic diagram of an artificial homogeneous long core.

156

157 **Table 3.** Fundamental characteristics of the core samples used in this work.

Flooding method	Core number	Length (cm)	Diameter (cm)	Permeability (mD)	Porosity (%)
	H_1	50.2	2.52	25.7	14.4
CO_2 flooding	H_2	50.4	2.52	51.8	16.7
	H_3	50.1	2.52	75.7	19.2

CO_2-SAG flooding	J_1	50.3	2.52	26.3	14.1
	J_2	50.1	2.53	50.1	17.1
	J_3	49.8	2.52	76.2	18.8

158

159 Core-flooding tests

160 The flow diagram of core flooding apparatus used in this study is shown in Figure 2. In this
161 arrangement, three core holders (Hongda, China, L=75 cm, T_{max}=130°C, P_{max}=80 MPa) are
162 positioned horizontally and connected in parallel in order to simulate a multilayer reservoir.
163 Process fluids (CO_2, live oil, and brine with $MnCl_2$ (Mn^{2+}, 15g/L)) were delivered
164 independently to the cores (Figure 2) using three separate high-pressure cylinders (Hongda,
165 China; T_{max}=130°C; P_{max}=80 MPa). The temperature of all core holders and tanks was ensured
166 by placing them in an oven (Hongda, China; T_{max}=120.0±0.1°C). Displacement of CO_2, crude
167 oil, and brine into the multilayer core system was implemented using a dual ISCO syringe
168 pump. A second pump was used to apply a constant confining pressure. A third pump was used
169 together with three back pressure valves to ensure that the backpressure was controlled and
170 constant. A set of gas-liquid separators and mass flow meters was used to measure the fluids
171 produced from each core. All data, including pressure and flow data were collected and logged
172 using a computer.

173

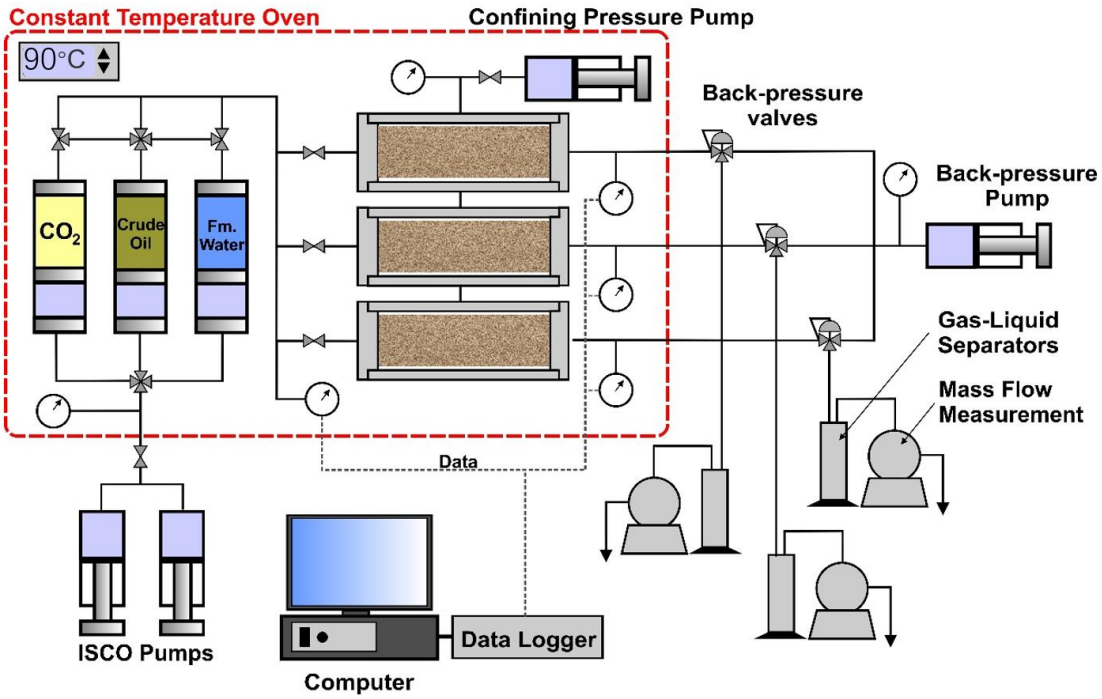

Figure 2. Schematic diagram of flooding experiments.

Conventional miscible CO_2 core flooding tests were carried out on cores H_1, H_2 and H_3 in the following two steps.

(1) The oven and the core-flooding flow rig it contains was raised to 90°C and kept at this temperature for 24 hours to ensure a constant starting temperature in all parts of the apparatus inside the oven and all process fluids. Cores H_1, H_2 and H_3 were cleaned and dried, and then placed in their core holders. Each core was subjected to separate evacuation for 24 hours. Brine with $MnCl_2$ was injected into each core, separately. A maximum of 30 HCPV of crude oil was then pumped into each core separately in order to attain the connate water saturations (S_{wc}) and initial oil saturations (S_{oi}) in each core. Subsequently, all core holders were left undisturbed for 24 hours in order to obtain equilibrium at reservoir conditions (90°C, 23MPa).

(2) A constant flow of CO_2 was injected at a rate of 18 cm^3/h (This injection rate is based on the oilfield injection rate and the previous experiments [10]. This rate will not lead to a rapid breakthrough of CO_2 BT, but a higher oil RF.) into all three cores at the same time from

the same inlet and at the same input pressure. The produced fluids from each core were collected and measured individually but at the same output pressure (23 MPa) using the back pressure pump and back pressure valves on each output line. The flow of CO_2 was stopped when there was no further oil production from the multilayer system. Steps (1) and (2) represent the core-flooding experiment using the conventional miscible CO_2 flooding process.

The miscible CO_2–SAG core flooding tests were carried out on cores J_1, J_2, J_3 using the following four steps.

(3) Step (1) was repeated, but using cores J_1, J_2, J_3.

(4) Step (2) was conducted on the cores J_1, J_2, J_3, but stopping the core-flood as soon as CO_2 breakthrough (BT) occurred. This CO_2 injection will be called the primary injection.

(5) All three core holders were isolated during the CO_2 soaking stage by closing all input and output valves. The length of time for this shut is a critical parameter which is discussed later in the paper.

(6) The input and output valves were reopened, and CO_2 injection was recommenced into all three cores at a constant flow rate of at 18 cm^3/h as in Step (4). This secondary CO_2 flood was continued until no further crude oil was produced.

The fluid volumes, injection pressures and production pressures and were monitored and recorded continuously during the entire flooding process. The asphaltene content of all produced oil was also measured.

Post-flooding tests

All the long cores were divided into 10 core plugs with the same length after flooding, the resulting short cores were subjected to NMR testing (Mini-MR, Niumag, China) to obtain the residual oil distribution by transverse relaxation time (T_2) spectrum analysis.

Asphaltene is soluble in aromatic hydrocarbons but not in alkanes. Other components of crude oil are soluble in alkanes. Consequently, *n*-heptane can be used to clean cores of their non-asphaltene oleic components[25]. In this work, the short cores were cleaned with *n*-heptane using the Soxhlet method (Soxhlet Extractor SXT-02, Shanghai Pingxuan Scientific Instrument CO., Ltd., China) which removed all oleic fluids remaining in the cores after flooding, but leaving the asphaltene precipitation blocking pore throats and adsorbed to pore walls. Methanol was used to remove any aqueous fluids remaining after the floods. Subsequently, all of the short cores were dried. Their gas permeability was then measured. This permeability was the permeability that had been affected by asphaltene precipitation both blocking pore throats and due to adsorption to mineral surfaces.

It should be noted that due to the non-polar nature of cyclohexane on asphaltene dissolution, cyclohexane reversal flooding can remove the asphaltene blocking pore throats. By contrast, reverse flooding using toluene can remove any asphaltene adsorbed on mineral surfaces. Cyclohexane reverse flooding was performed (flow rate =30 cm^3/h until a stable differential pressure was sustained) to measure any formation damage that had accrued from the mechanical blocking of pores and pore throats[15]. It was found that this process removed asphaltene due to mechanical blockage of pore throats in all cores. The cores were then cleaned, allowing the decline in permeability decline associated with asphaltene pore throat blockage to be quantified.

Subsequently, the cores were subjected to reverse flooding with toluene[16], in order to remove adsorbed asphaltenes that could not be removed with cyclohexane. The cores were then cleaned again, and the permeability was remeasured in order to obtain the permeability decline due to the adsorption of asphaltenes directly to mineral surfaces.

Results and Discussion

Differential pressures (ΔP)

Figure 3 shows that the dynamic trend of the ΔP values during CO_2 and SAG flooding are very similar during the continuous CO_2 injection before CO_2 BT. The similar behavior is attributed to the matched physical properties of the two groups of cores composing the three-layer system (see Table 3), and suggests that their similar petrophysical properties result in similar distributions of fluids at the start of the experiment and progressively during initial CO_2 flooding.

In the SAG flooding process, the CO_2 soaking stage was started after the CO_2 BT (occurring at 0.4961 PV), and then the secondary CO_2 flooding was performed (until 1.192 PV). During the CO_2 soaking stage, the crude oil that had not previously interacted sufficiently with CO_2 had the opportunity to adsorb CO_2. As a consequence, the volume of this crude oil expanded and its viscosity decreased, leading to the redistribution of fluids within the pores. The saturation of the oil in the pores that had composed the well-connected and larger pore size gas channels formed by the initial CO_2 flooding increased. Consequently, the displacement resistance of SAG secondary flooding was greater than that during CO_2 flooding at same injected CO_2 volume, and less than that before CO_2 BT. The secondary CO_2 BT occurred more quickly due to the higher gas saturation and lower oil viscosity in the rock at the beginning of the secondary flooding. It is worth noting that the CO_2 BT only occurs in the high permeability layers during CO_2 flooding and SAG flooding. There is no obvious CO_2 BT in the medium and low permeability layers, and the displacement front of CO_2 flooding does not advance to the outlet end.

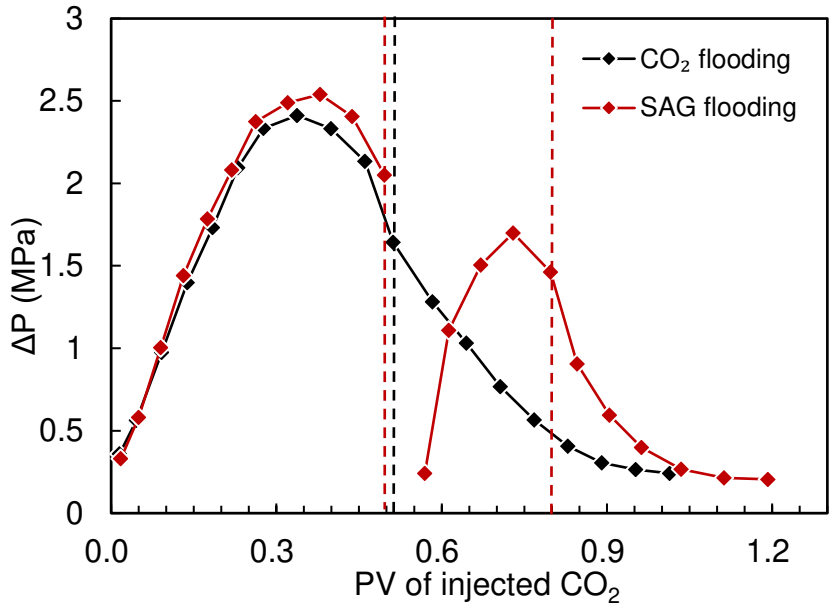

Figure 3. Measured differential pressure (ΔP) during CO_2 flooding and SAG flooding. Vertical dashed lines show CO_2 BT for each flood.

Pressure decay during the CO_2-soaking process

Figure 4 shows that the core fluid pressure declines rapidly as soon as the CO_2-soaking process begins, becoming progressively slower. The pressure-time curve can be approximated by a power-law, fits of which are also shown in the figure. This behavior arises from (i) dissolution of gas in the oil near the gas-oil interface, and (ii) gas diffusion deeper into the oil. Both of these processes depend on the partial pressure of gas already in the oil. As a result, dissolution becomes progressively less efficient until a steady-state is reached[26-27].

In our case, the cores were soaked in brine and cleaned before the laboratory experiments were carried out. This process makes the cores water-wet, with water preferentially coating the surfaces of rock grains and completely filling the smallest pores. By contrast, crude oil and CO_2 are non-wetting phases. Such non-wetting phases occupy the center of large and medium-sized pores and pore throats as far from the mineral surfaces as possible. The injected CO_2 prefers to be in contact with the crude oil in the center of the large pores and throats. Under these conditions, we expect that the initial swift pressure drop occurs as the result of efficient

dissolution of gas in oil with which it is in direct contact. Once the partial pressure of CO_2 within this oil approaches saturation, further decay will be controlled by gas diffusion within the oil[28-29]. However, gas diffusion through oil in small pores and between pores with small pore throats will be slowed down by the greater tortuosity of the oil pathways through which the gas must diffuse. The process of gas diffusion is therefore relatively slow[30-31]. As a consequence, there exists an optimal soaking time (T_c) at which the dissolution of CO_2 in oil is maximized, allowing the oil to swell and develop greater mobility, while avoiding slow pressure decay stage. This T_c is exhibited as an inflexion in the pressure decay.

The determination of the T_c value can improve the efficiency of SAG flooding in oilfield development. Usually, a pressure decay rate threshold value is established, and the soaking stage is stopped when the decay rate is lower than this value. For example, in the results of this experiment, when the pressure decay rate in the core J_3 is lower than 1 MPa/h (the pressure decay of J_3 is the slowest among the three cores), T_c=2 h. When threshold value is applied in oilfield development, the threshold value should be determined according to the specific characteristics of the reservoir and the characteristics of pressure attenuation.

The greater the permeability, the greater the pressure decay rate. This is due to there being less residual oil in the high permeability core at the beginning of the soaking stage, as well as to the fact that the higher the CO_2 saturation, the larger the contact area between CO_2 and the fluid in the core, and the better connectivity between the pores, the faster the diffusion of CO_2 in the fluid in high-permeability core. By contrast, the lower the core permeability, the poorer the connectivity between the pores, the lower the pressure decay rate, and the lower the final equilibrium pressure, the greater the T_c value. Such a scenario is an indicator that lower permeability cores require longer soaking times in order for the process to be effective.

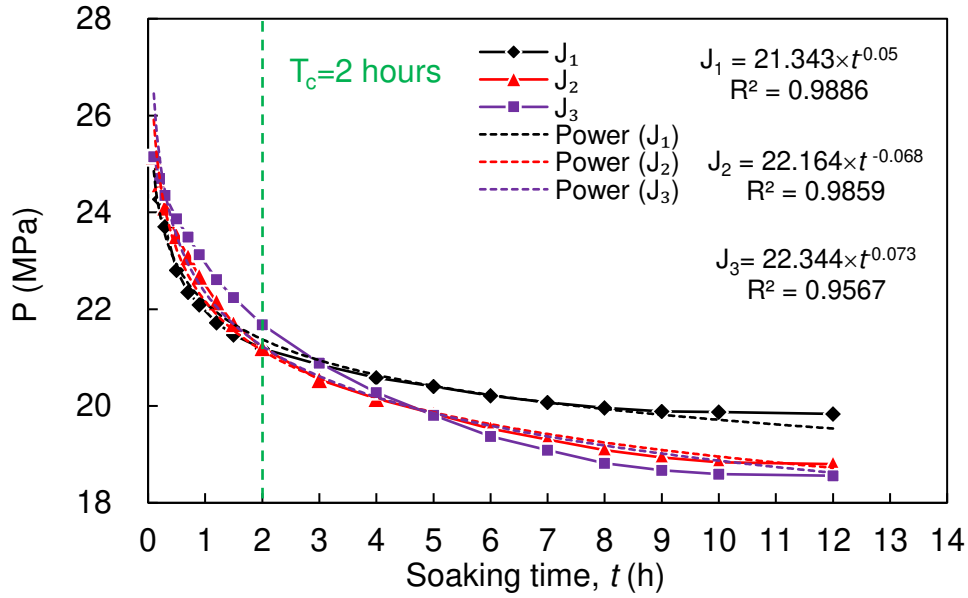

313

314 **Figure 4.** Measured CO_2 pressure in the core plugs with respect to soaking time *t*, with best-
315 fit power laws.

316

317 Oil recovery and produced fluids

318 Figure 5 and Table 4 show that the dynamic production of crude oil during the two flooding
319 processes had similar characteristics up until CO_2 BT. The high-permeability layer had the
320 highest oil RF as well as the fastest increase in RF. The fractional oil production (FOP) of high
321 permeability layer is the largest, and gradually increases, while the FOP of medium and low
322 permeability layers decreases gradually. This is because the high permeability layer presents
323 the smallest capillary resistance, the resistance of CO_2 flooding is small, and as the
324 displacement front advances faster in the high permeability layer, this displacement resistance
325 becomes smaller[32]. The difference in displacement resistance between layers with smaller
326 permeabilities is greater. A larger proportion of injected CO_2 enters the high-permeability layer.

327

328 It is worth noting that there is a large difference between the ratio of the FOP of each layer
329 (67:25:8) and the ratio of the initial permeability (75:52:26), which means that a relatively small
330 difference in initial permeability would result in a huge difference in the FOP. In other words,
331 the influence of the initial permeability difference on the oil production effect is magnified

upon CO_2 injection. The oil RF of the high, medium and low cores increased little (by 6.8%, 3.4%, and 1.7%, respectively) after CO_2 BT during CO_2 flooding, even after a large volume of CO_2 is continuously injected (Table 4). The oil production after CO_2 BT mainly comes from high permeability layers. The oil production at this time depends mainly on the extraction of CO_2 on oil, and the utilization efficiency of CO_2 is very poor[33].

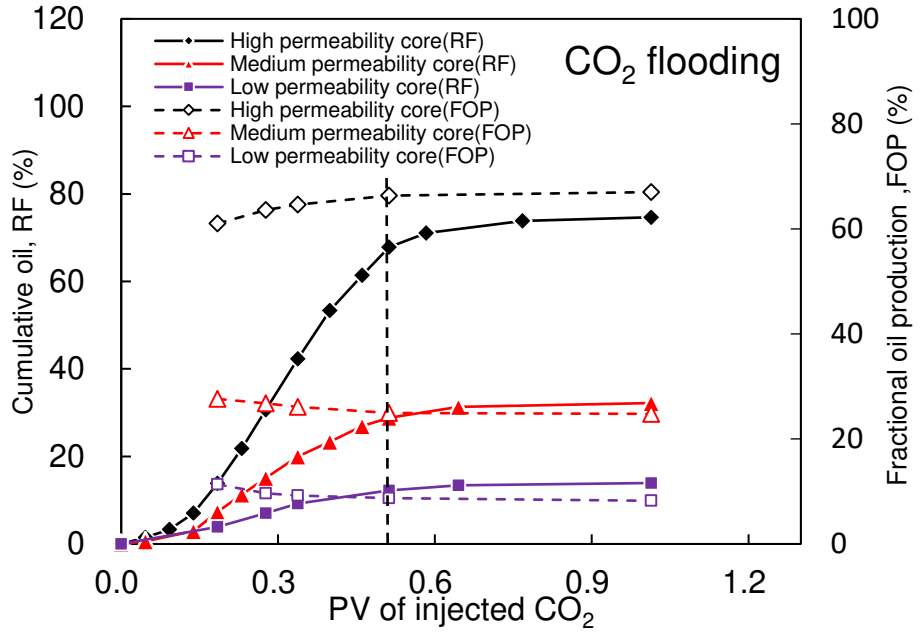

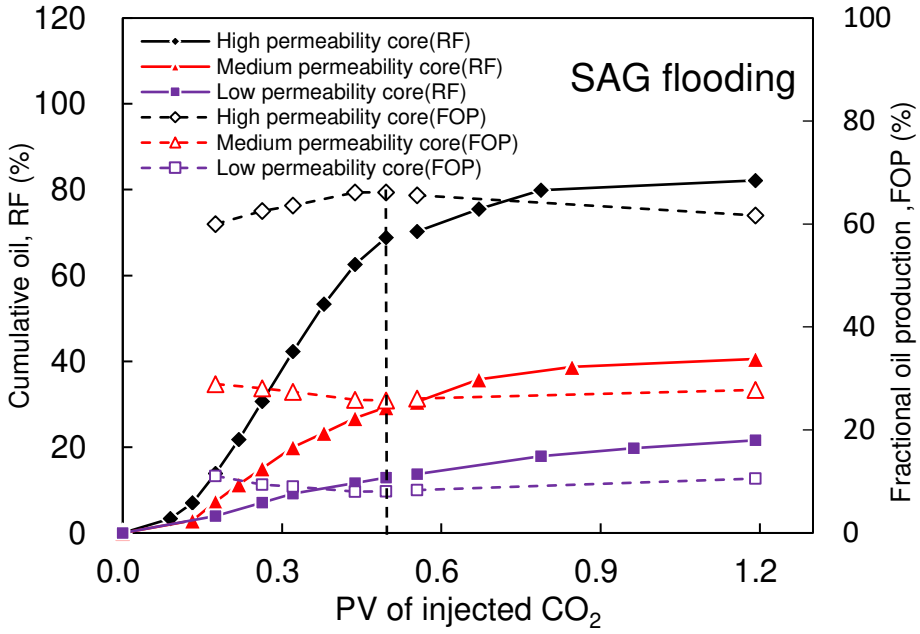

Figure 5. The cumulative oil RF and FOP of each long core. The vertical dashed line shows the CO_2 BT at the end of the preliminary flood.

Table 4. Oil RF and FOP of each long core.

Flooding method	Timing	Oil RF %			Oil FOP %		
		High	Medium	Low	High	Medium	Low
Simple CO_2	At CO_2 BT	67.8	28.8	12.2	66.4	24.9	8.7
	At flooding end	74.6	32.2	13.9	67	24.8	8.2
	$\Delta RF_1 \backslash \Delta FOP_1$	6.8	3.4	1.7	0.6	-0.1	-0.5
SAG	At CO_2 BT	68.9	29.4	12.9	66.2	25.7	8.1
	At flooding end	82.2	40.5	21.6	61.6	27.7	10.6
	$\Delta RF_1 \backslash \Delta FOP_1$	13.3	11.1	8.7	-4.6	2	2.5
SAG-Simple CO_2	$\Delta RF \backslash \Delta FOP$	7.6	8.3	7.7	-5.4	2.9	2.4

ΔRF_1= Oil RF at flooding end-Oil RF at CO_2 BT

ΔFOP_1= Oil FOP at flooding end-Oil FOP at CO_2 BT

ΔRF= Oil RF at flooding end (SAG)-Oil RF at flooding end (Simple CO_2)

ΔFOP = Oil FOP at flooding end (SAG)-Oil FOP at flooding end (Simple CO_2)

During the secondary flooding process after the soaking stage in SAG flooding, the cumulative recovery of each layer continued to increase, and the increased RF was 13.3%, 11.1%, and 8.7%, respectively (Table 4). Compared with CO_2 flooding, the medium and low permeability cores attained relatively higher improvements in oil production, while the FOP of these layers also increased after CO_2 BT. This is due to the soaking stage alleviating the problem of inadequate contact between CO_2 and crude oil in the low and medium permeability layers. We observe, particularly, that the high permeability layer has the best oil production improvement after the soaking stage, while the FOP is reduced, indicating strongly that SAG not only improves effectively the RF of the overall multi-layer system, but can also improve effectively the oil production in low and medium permeability layers, reducing the difference in oil production in each layer caused by the difference in initial permeability.

We found that the final oil RF of each layer of SAG flooding is 7.6%, 8.3%, and 7.7% higher than that of CO_2 flooding, i.e., approximately the same improvement for all of the layers, irrespective of their petrophysical properties (Table 4). Moreover, the difference in the FOP of each long core is, relatively speaking, smaller, which indicates that in the multi-layer reservoirs with different permeability CO_2-SAG flooding is generally more effective than miscible CO_2 flooding in displacing oil, helping to tap the oil production potential of medium and low permeability layers.

Figure 6 shows the progression of the conventional CO_2 flooding process and the CO_2-SAG flooding process. In both cases the initial state is shown on the left-hand side of the figure and injected CO_2 flows from left to right. The figure does not include changes due to asphaltene precipitation or pore blocking. The rock is assumed to be water-wet, and formation water is shown in blue. Oil is shown in two shades of green, according to whether it is accessible or trapped. For the purposes of this discussion 'accessible oil' is that which is mobile under normal CO_2 flooding conditions. This implies that the fluid pressure differences during flooding are greater than the capillary pressures retaining the oil in the pores, and further implies that accessible oil is to be found in the larger pores, and these pores are also linked by larger pore throats. By contrast, 'trapped oil' is that which occupies the smaller pores or pores only accessed by small pore throats. These oil accumulations are subjected to capillary pressures which are too high for them to be moved by the normal process of CO_2 flooding.

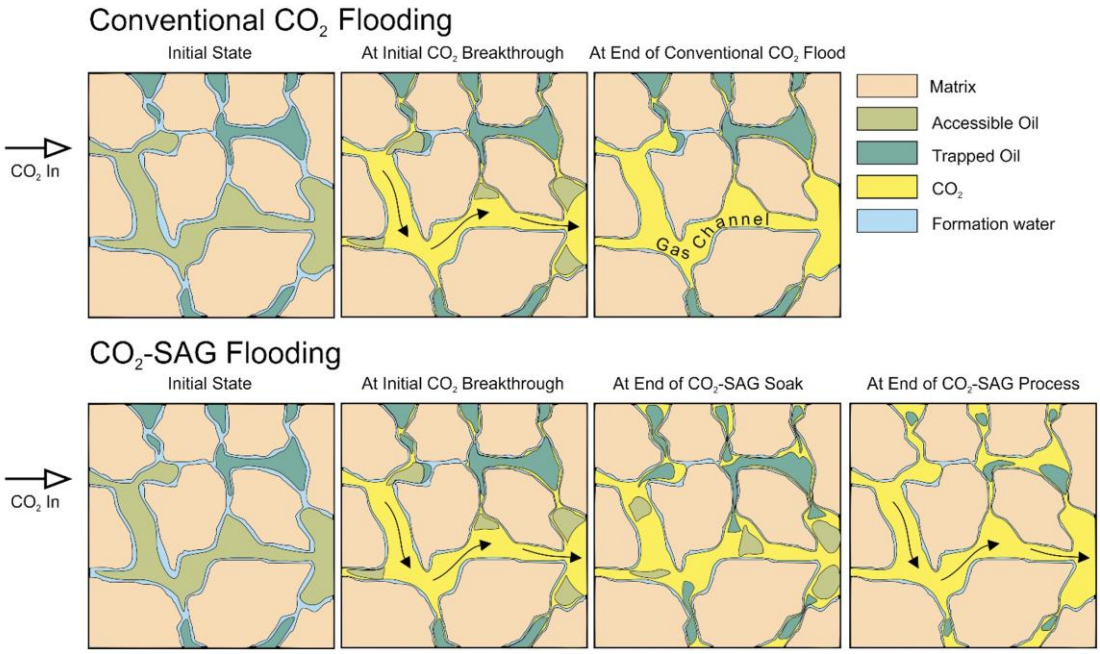

Figure 6. The progression of conventional CO_2 flooding and CO_2-SAG flooding processes exemplified using a microstructural/microfluidic model.

In the case of conventional CO_2 flooding process, injected CO_2 is not the wetting fluid. It preferentially moves through pores with lower capillary pressures, either displacing oil or occupying space between the oil and undisplaced oil. Since CO_2 has a much lower density and viscosity than either oil or water, it is able to penetrate into small pores, even if it has little ability to displace the oil from them. Consequently, by the time the CO_2 has broken through (centre top panel of the Figure 6), there are three observations (i) CO_2 has displaced (and produced) a large proportion of the accessible oil in the large pores, (ii) the flooding pathway now predominantly contains gas, and this gas channel has a high permeability, which by-passes oil in the remainder of the rock, and (iii) a small amount of residual accessible oil exists, for which production depends on a marginal interplay between flooding pressures and the capillary pressure. If flooding progresses after breakthrough, these final accumulations of oil will be eventually produced (top left panel of the Figure 6).

In the case of CO_2-SAG flooding, the story up until CO_2 breakthrough is the same as described previously. During the soaking procedure, the remaining accessible and trapped oil undergo

two changes. First, the oil expands as CO_2 dissolves in the oil. The limited space in pores implies that some of the oil moves in response the subsequently increased fluid pressures. Second, solution of CO_2 in the oil also reduces the oil viscosity, making it more mobile. The result of these two effects results in the remaining accessible oil and some of the trapped oil extruding towards and into the high permeability gas channel. This situation is shown in the bottom third panel from the left. The presence of the CO_2 around the oil has changed its properties and brings the oil towards the high permeability channel. The promotion of oil RF by the miscible effect requires a certain amount of time and space for the interaction of CO_2 and crude oil, the soaking stage provides longer time of interaction. The second CO_2 flood is now capable of producing the more mobile extruded oil (bottom right-hand panel in the Figure 6).

The asphaltene content of the produced crude oil decreases rapidly before CO_2 BT, as shown in Figure 7, with the production of crude oil, while the asphaltene content in the produced oil in the initial stage remained at 90%, and this part of the crude oil hardly came into contact with the injected CO_2. There is an increase in the CO_2 dissolved in the crude oil as the displacement front progresses, which leads to increased asphaltene precipitation in the core and less asphaltene in the produced oil.

The asphaltene content of the produced oil after soaking was found to be smaller than that for miscible CO_2 flooding at the same amount of injected CO_2. This may be ascribed to the larger amounts of CO_2 dissolved in the residual oil as a result of the soaking process, resulting in greater asphaltenes precipitation, more asphaltenes are deposited in the core during SAG flooding.

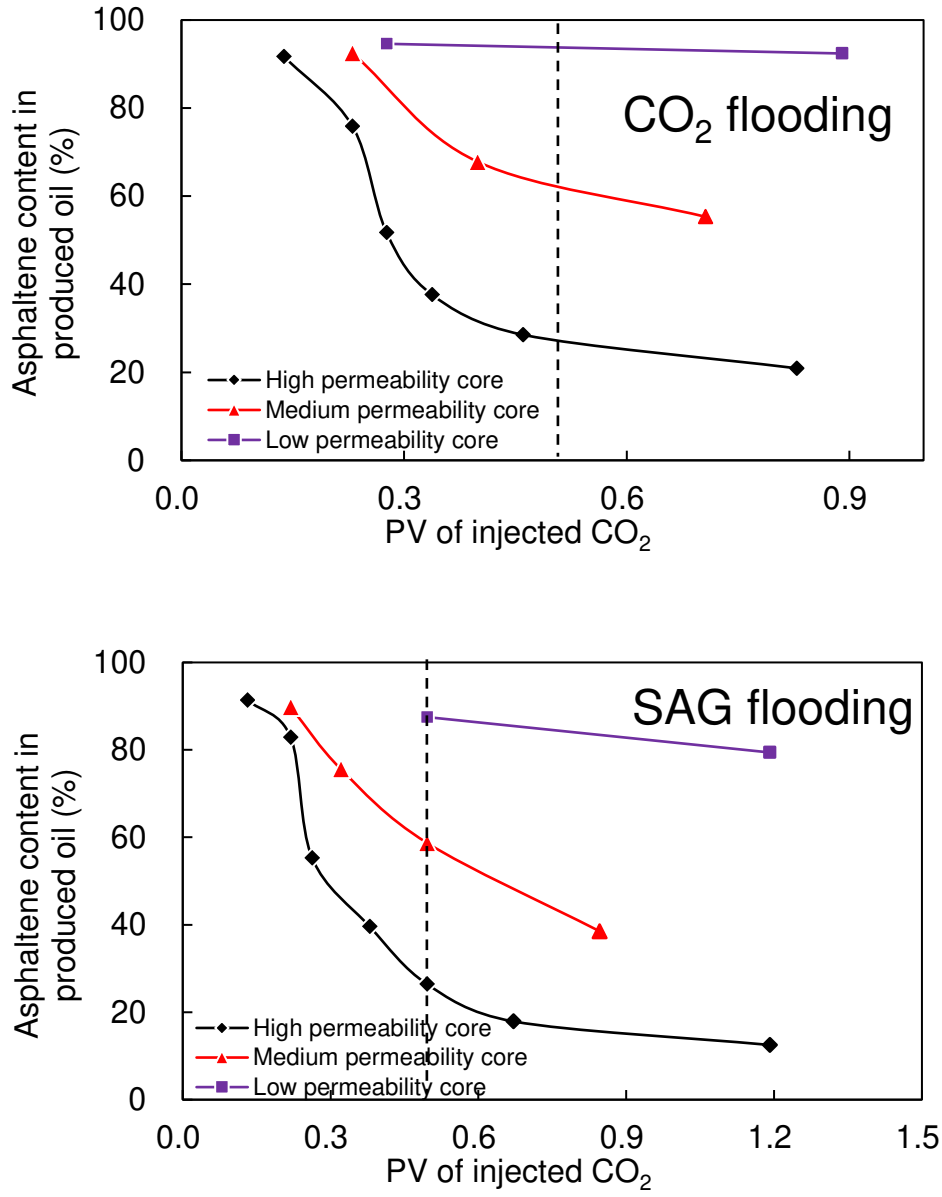

Figure 7. Asphaltene content in produced oil and PV of injected CO_2 during flooding.

Oil RF distribution

The NMR spectrometry provides the T_2 relaxation time signal amplitude of the oil in each short core plug (long cores are cut equally) after the experiments[34]. The oil RF of the cores at different locations was calculated according to the volume of produced oil, saturated oil, and the total intensity of the residual oil signal amplitude (Figure 8).

The oil RFs in the high permeability long core after conventional CO_2 flooding (Figure 8 upper panel) decreases gently along the injection direction. However, the oil RFs towards the middle (L=22-27 cm) of the medium permeability layer exhibits a large variation, and the oil RF distribution along the injection direction is divided into two parts with gradual decrease, which may be attributed to the displacement front staying in this part of the rock (L =22-27 cm) rather than advancing to the outlet at the end of the displacement by the development of fingering sufficient to ensure at least one gas channel breaks through. The same observation occurs at L =12-17 cm in the low permeability long core, but this variation is smaller. For the medium and low permeability cores there is little variation of the oil RF in the latter half of the core, implying that the crude oil in the core with L >17 cm is not driven directly by CO_2. Compared with the medium permeability long core, the displacement front in the low permeability long core is closer to the injection end.

For CO_2-SAG flooding, the oil RFs in each long core is large than that after conventional CO_2 flooding (Figure 9 lower panel). The curve variation (L =17-32 cm) also appears in the high permeability layer. However, the soaking stage causes this variation to become flat, but the variation range becomes larger. There are two trends in the distribution of oil RF in high permeability layer. The pattern of oil RF in the rocks towards the injection end is relatively uniform, and varies little. The amount of oil RF near the outlet end shows an obvious gradual downward trend along the injection direction, and shows that the soaking process improves the efficiency of the residual oil at the injection end and middle being driven out during the secondary displacement process.

If the position of the displacement front in the same permeability core after CO_2 flooding is compared to that after SAG flooding, we observe that the displacement front in the low and medium permeability layers is not advanced significantly during secondary flooding as a result of the soaking stage. The soaking does not significantly expand the CO_2 sweept volume, but

only enhances the CO_2 displacement effect in the core pores that have been swept by CO_2 before CO_2 BT.

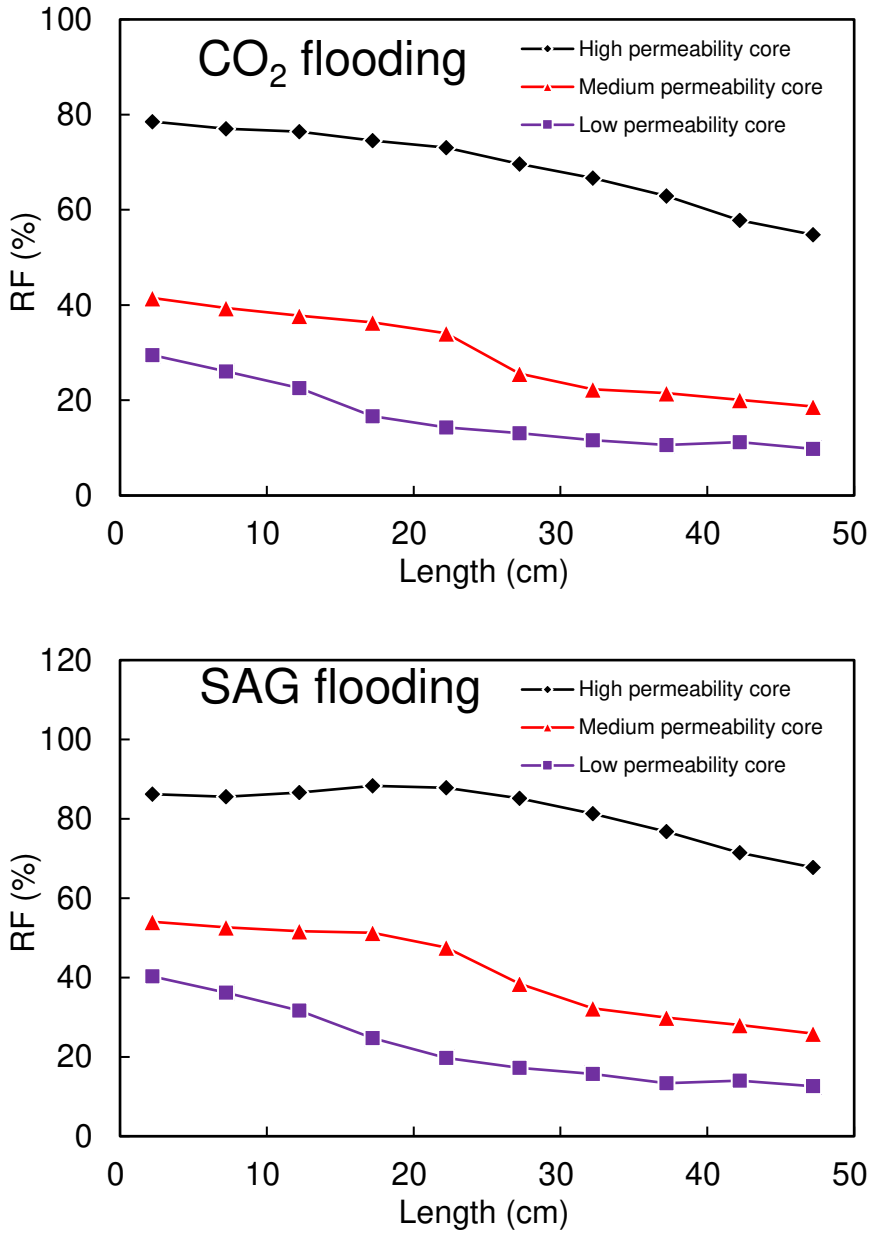

Figure 8. Oil recovery calculated according to the signal amplitude in T_2 spectrum by NMR tests along the cores.

The distribution of the difference between the final oil RF of the two floods is shown in Figure 9. The parameter ΔRF (ΔRF(%) = RF (SAG)−RF (CO_2)) represents the degree of improved oil

production of SAG flooding compared to conventional CO_2 flooding. For the high permeability long core, the improvement in oil production along the injection direction gradually increases, reaches a maximum value in the middle (L =27 cm), and then slightly decreases. The improvement in RF that occurs during the soaking stage is controlled by several factors, (i) the amount of residual oil at the start of the soaking phase, and (ii) the amount and distribution of CO_2 retained in the pores at the beginning of the soaking.

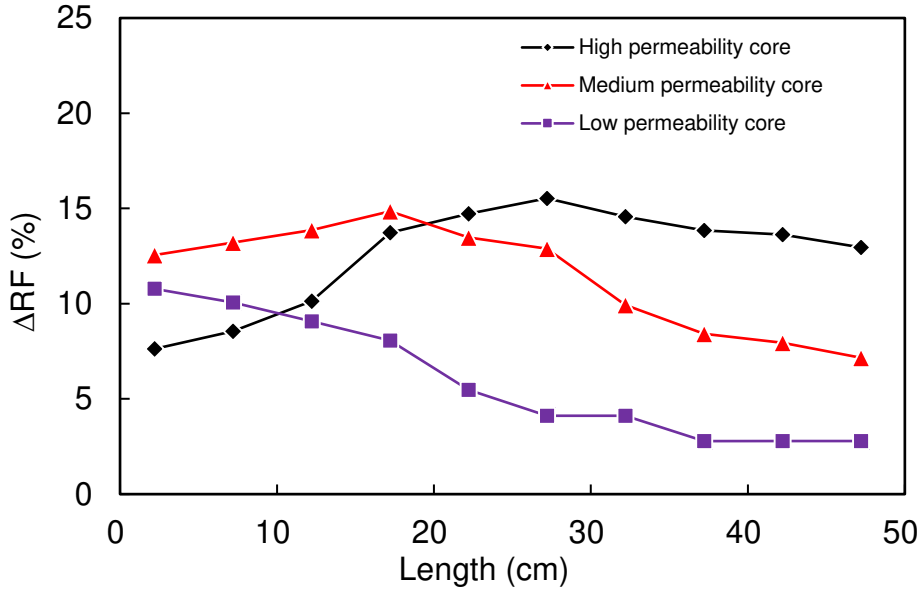

Figure 9. The difference in oil RF between the flooding processes as a function of length along the cores.

Proximally to the injection end, there is a larger saturation of retained CO_2, but production from this zone has been good (at least for the high permeability core), so there is only a small amount of residual oil. Consequently, there is less scope for the soaking process to be effective, which leads to values of ΔRF = 7.62% for the high permeability core. However, more residual oil is present for the low and medium permeability cores, which results in a larger improvement in recovery factor (ΔRF = 12.55%, ΔRF = 10.78%, respectively); the medium permeability core performing better than the low permeability core because it allows access to more CO_2.

The amount of residual oil at the start of the soaking phase gradually increases along the injection direction, but the amount of CO_2 retained at the beginning of soaking gradually decreases. Consequently, the central portions of the high and medium permeability long cores provide the best oil production enhancement and hence the greatest ΔRF (about 14.85% and 15.53%, respectively). The low permeability core does not exhibit this behaviour because its low permeability reflects the fact that its pores are sufficiently small that even though a large saturation of residual oil is retained after initial flooding, there is little invasion of CO_2 to enable much of it to be produced after soaking.

The values of ΔRF fall again towards the output end of each long core, reflecting that although the retained oil saturation is high, the CO_2 saturation is low. It is here that there is the greatest difference between the three different permeability long cores, with the greatest improvement occurring for the high permeability long core (ΔRF=12.96%).

In summary, the soaking stage leads to an overall improvement in the recovery factor for cores of all permeability and at all locations, but the best improvements were in the middle of the medium and high permeability cores (around 15%) and proximally to the injection end of the low and medium permeability cores (around 12%).

Permeability damage

We defined a permeability decline parameter as K_d after flooding ($K_d = 100 \times (K_b - K_a)/K_b$, which is reported as a percentage, and where K_b is the pre-flooding permeability of the core and K_a is permeability of the core after flooding, Figure 10).

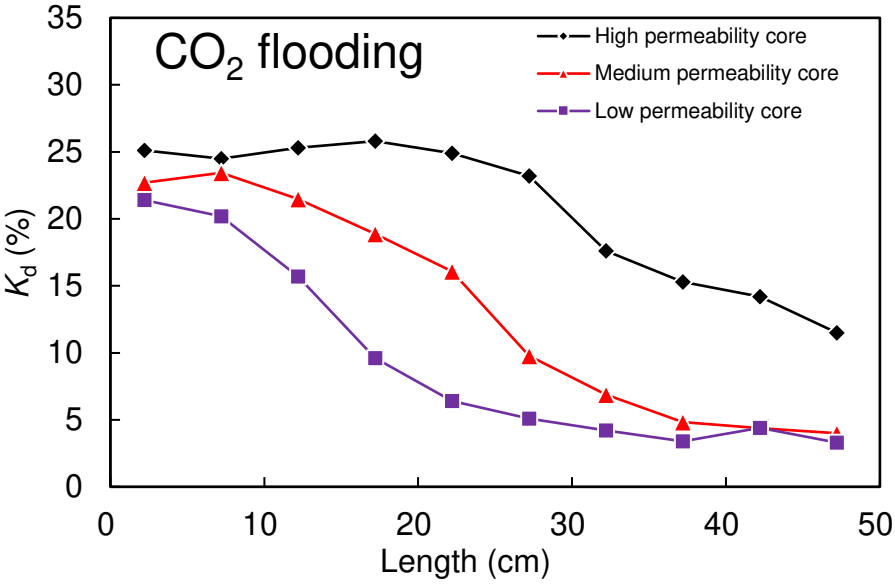

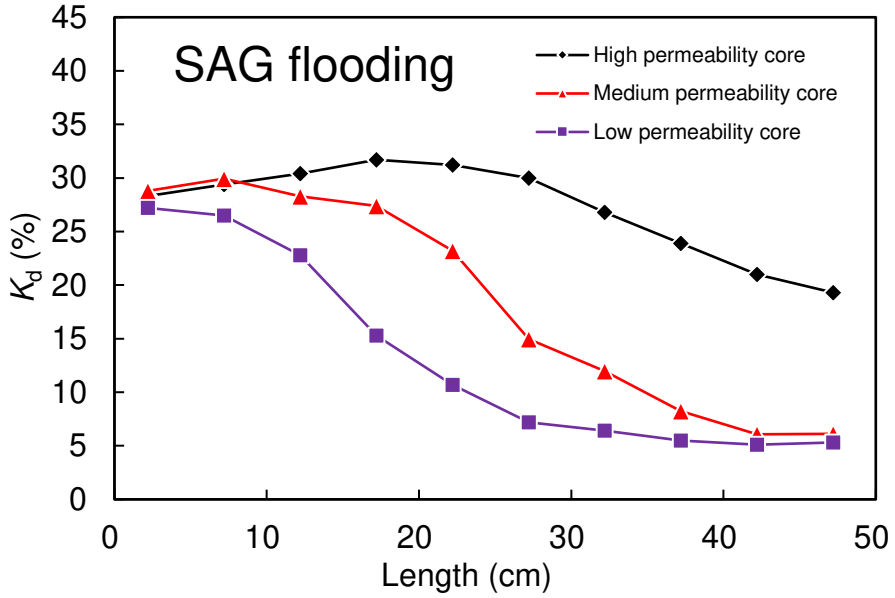

Figure 10. The spatial distribution of the reduction in permeability along the cores due to precipitation of asphaltene.

It would be expected that permeability decline is associated with the precipitation of asphaltene which reduces the water wettability of the rock as well as blocking flow pathways . It has been hypothesized[10] that the amount of permeability reduction is controlled by (i) the extent of the precipitation of asphaltene, (ii) the efficiency of asphaltene particle migration (initial permeability of the rock which depends on its pore microstructure), and (iii) the efficiency with

526 which such particles can block pore-throats. We also recognize that cores and reservoir
527 formations with higher oil recovery factors have, hosted the passage of more CO_2 during initial
528 flooding. It would therefore be expected that these rocks would be more likely to exhibit
529 increased asphaltene precipitation and hence a greater decline in permeability[37-38].
530
531 After conventional CO_2 flooding, the permeability near the injection end (L=0-27 cm) of the
532 high permeability long core underwent a reduction of about 25%. Moving more distally from
533 the injection face, the degree of permeability reduction decreases until it is 11.5% at the output
534 face (Figure 10 top panel). This pattern of permeability damage is the result of the continuous
535 advancement of the CO_2 flooding front, the continuous solution of CO_2 in the crude oil, the
536 consequent formation, precipitation and migration of asphaltene particles, followed by the
537 adsorption of asphaltene onto grain surfaces and their blockage of pore throats.
538
539 The permeability decline of the medium and low permeability long core follows a similar
540 pattern, but undergoes a slightly smaller permeability reduction at the injection end (about 23%
541 for L=0-7.5 cm), but then steadily declines until the permeability reduction only about 4% at
542 the output face.
543
544 It is clear from Figure 10 that CO_2-SAG flooding causes greater damage to permeability than
545 conventional miscible CO_2 flooding for all positions along all three cores. The SAG flooding
546 process provides a similar pattern of permeability reduction for all locations in all three long
547 cores. This is because during the soaking process larger amounts of CO_2 are dissolved in the
548 residual oil, which leads to a concomitant increase in asphaltene precipitation, and which then
549 narrows and blocks pore throats more effectively[35-36]. This view is supported by the decrease
550 in the amount of asphaltene in the produced oil compared to that in the initial oil(Figure 7).
551 Previously[10] it has been noted that, the pattern of permeability decline along the cores was
552 smoother for CO_2-SAG flooding compared to CO_2 flooding, and this has been associated with
553 the soaking leading to a more homogeneous precipitation of asphaltene.

It is possible to quantify the percentage difference in K_d between the two flooding processes[10] using $\Delta K_d(\%) = K_d(\text{SAG}) - K_d(CO_2)$, which is shown in Figure 11.

The ΔK_d value in the high permeability layer increases in the direction of injection. The closer to the outlet end, the more residual oil at CO_2 BT. Compared with CO_2 flooding, the additional precipitation of asphaltene associated with the soaking stage of the CO_2-SAG process is greater, and the asphaltene precipitation during the secondary flooding process has a relatively large impact on the core permeability at the outlet end.

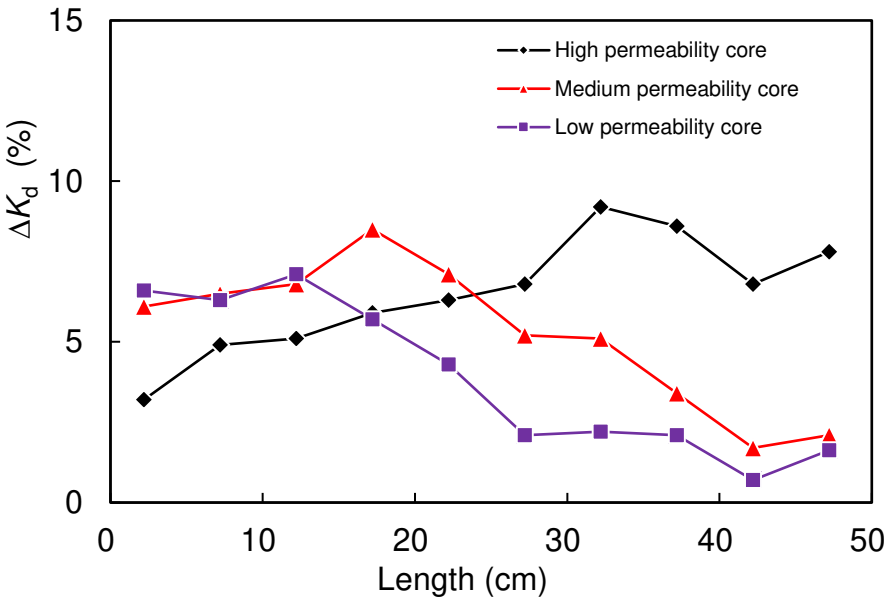

Figure 11. The difference in permeability decline (ΔK_d) between the two flooding processes.

The distribution trend of ΔK_d in the low and medium permeability long cores decreases along the injection direction, which is exactly the opposite of the trend of ΔK_d distribution in the high permeability long core. This also suggests that interaction of CO_2 and oil during the soaking stage occurs mainly in the pores swept and affected by injected CO_2 before CO_2 BT, that is, in the core near the injection end in low and medium permeability long cores. The processes of

572 CO_2 soaking and secondary flooding increased the permeability decline of these cores, and did
573 not have a substantial influence on the reduction in the permeability of the cores near their
574 outlet end.
575
576 The ΔK_d of the cores proximal to the injection face in the medium and low permeability cores
577 is higher than the ΔK_d near the injection face of the high permeability long core. The significant
578 additional permeability decline near the injection face in the low permeability core is worthy
579 of attention, and corresponding measures should be taken at the corresponding injection well
580 during the SAG flooding process. It shows that CO_2 soaking and secondary flooding has a
581 substantial influence on the permeability decline of the injection end and middle in medium
582 permeability long core, while only affects ΔK_d at the injection end in low permeability. It also
583 shows that the CO_2 soaking and secondary flooding have a weak propulsion effect on the
584 displacement front, but it significantly increases the permeability decline of the cores that has
585 been swept by CO_2 at CO_2 BT. In short, the distribution characteristics of ΔK_d and ΔRF are
586 basically similar.
587
588 In this work we confirm the earlier observation[10] that CO_2-SAG flooding produces greater
589 permeability damage and a higher oil recovery factor than simple miscible CO_2 flooding. As
590 before[10], we have used a single parameter (K_{dp}) to take account of both oil recovery
591 improvement and permeability damage. Here, $K_{dp} = K_d/RF$ measures the amount of
592 permeability decrease, or damage, per unit increase recovery factor, and is shown for both
593 flooding processes in Figure 12.
594
595 The K_{dp} value of the high permeability core is the smallest, and the K_{dp} value of the low
596 permeability long core is the largest. This indicates that the large permeability not only leads
597 to high oil recovery, but also weakens the decline in permeability resulting from precipitation
598 of asphaltene. It is clear that high initial permeabilities are relatively insensitive to permeability
599 decline caused by both adsorption of asphaltene precipitation and blockage of pore throats by

asphaltene particles. The value of K_{dp} in the high permeability core changes only slightly along the injection direction, while its value shows a marked decrease in the flow direction for the low and medium permeability cores.

These observations arise because the gasflood front has advanced as far as the outlet face in the high permeability long core but has only advanced partially along the other two cores even though viscous fingering ensures that breakthrough has occurred. The value of K_{dp} falls rapidly in the vicinity of the flood front, which occurs at approximately 20±7 cm and 27±7 cm for the low and medium permeability cores, respectively. As a consequence, it may be said that although some oil is produced from the injection end of the low and medium permeability long core, damage to the core permeability is more significant than for the high permeability core.

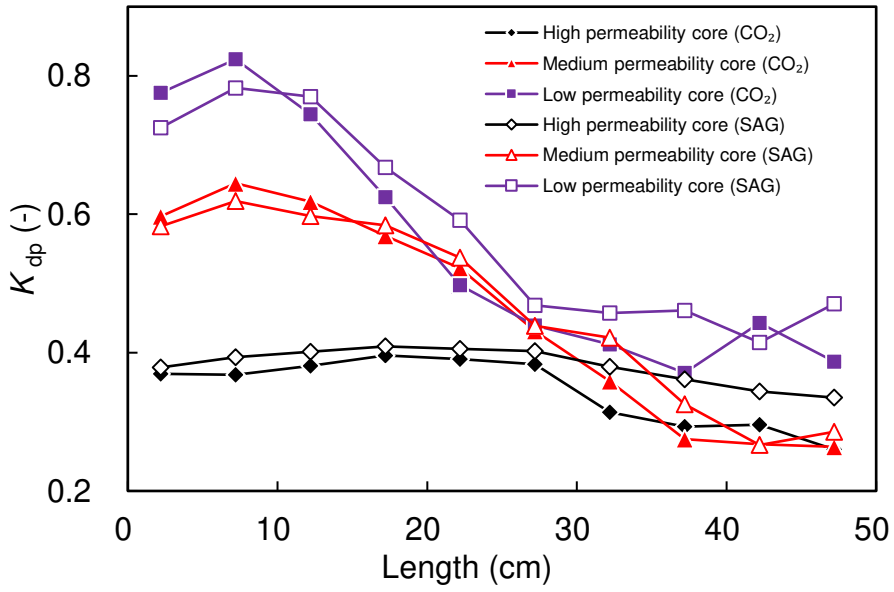

Figure 12. The distribution of the K_{dp} value along cores after flooding. The K_{dp} parameter represents the percentage permeability decline per unit increase in recovery factor, and for which large values are worse than small values.

In the high permeability long core, the difference in K_{dp} after CO_2 flooding and SAG flooding only exists in the cores near the outlet end, which shows that although the CO_2 soaking and

secondary flooding at the outlet end have effectively improved the oil production effect, they have caused relatively greater damage to permeability. Also, compared with CO_2 flooding, the improvement in oil production of SAG flooding in the middle cores is less than the damage to permeability.

Blockage and adsorption of asphaltene precipitation

The permeability decline due to adsorption and blockage effects of asphaltene precipitation can be separated in order to calculate the two kinds of decline percentage values through cleaning and flooding after the flooding experiments using special solvent (the cleaning process and calculation are shown in the "Post-flooding tests" section)[39].

Figure 13 shows the decrease in permeability caused by asphaltene precipitation blockage of pore throats after flooding ($K_{db=}100\times(K_{abc}-K_a)/K_b$), where K_{abc} is the permeability after the sample has only been cleaned of blockages. The parameter K_{da} is the decrease in permeability caused by asphaltene precipitation adsorption ($K_{da=}100\times(K_{afc}-K_{abc})/K_b$), where K_{afc} is the permeability after the sample has been fully cleaned of blockages and adsorbed precipitation. It will be noted that $K_d=K_{db}+K_{da}$. In addition, we define $R_b=100\times K_{db}/K_d$, which represents the percentage of permeability decline caused by asphaltene particle blockage with respect to the total permeability decline (Figure 14). Here, $R_a=100-R_b$ is the fractional decrease in permeability caused by the adsorption of asphaltene with respect to the total permeability decline.

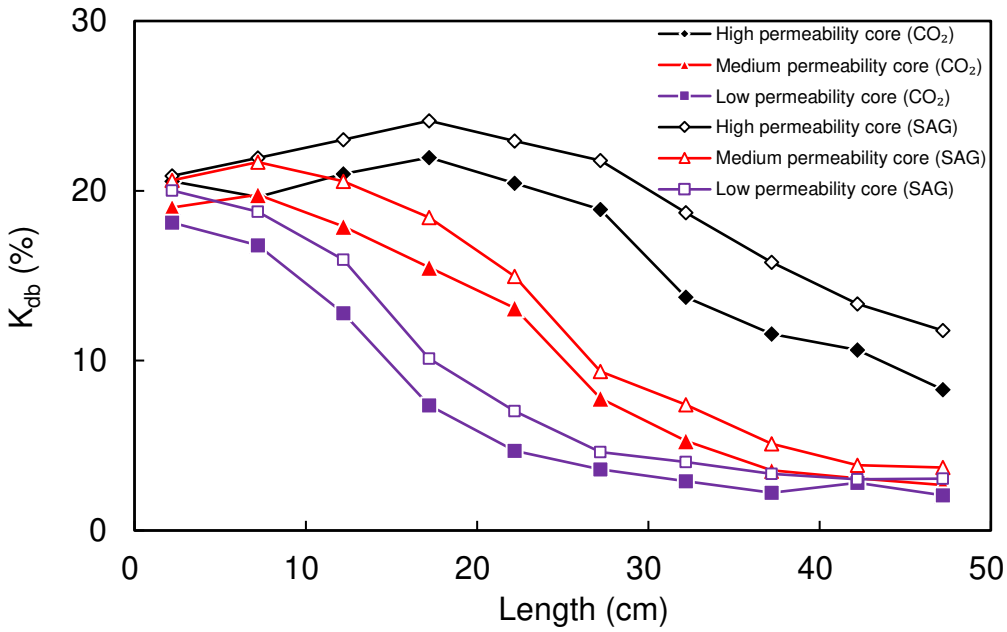

641
642 **Figure 13.** The distribution of the reduction in permeability due to asphaltene pore blocking
643 along cores after flooding, quantified by K_{db}, where small values represent small effects from
644 the pore blocking mechanism.

645

646 It is commonly considered[40-41] that the degree of asphaltene precipitation required to block
647 pore throats is related (i) to the overall extent of asphaltene precipitation, (iii) the asphaltene
648 particle size distribution, and (iii) the asphaltene particle mobility, all of which are inter-
649 dependent. The longer the migration distance of the fluid carrying asphaltene precipitation in
650 the pore throats, the greater its velocity, the longer the flooding time, the smaller the size of the
651 pore throats, and the more fluid that flows through the pore throat, the higher probability the
652 pore throat will be blocked, the more serious the blockage will be[42]. However, in the same
653 core, the permeability decline caused by asphaltene precipitation adsorption is only related to
654 the scale of asphaltene precipitation. Moreover, small particles have less ability to block pore
655 throats, but are very mobile (Stokes law), while large particles block pores throats easily but
656 are less mobile[43].

657

658 Figure 13 shows that the fall of permeability caused by the asphaltene particle blockage in each
659 layer at the injection end is similar. The high permeability core has low resistance to CO_2 flow

resulting in more CO_2 being injected, which in turn leads to the deposition of more asphaltenes. Hence, it would be expected that the permeability decline caused by blockage should be greater for this high permeability core than the other cores, which is not observed. It is possible that the initial large permeability of the rock protects it from permeability damage even if there is a greater deposition of asphaltene[6]. By contrast, the lower permeability cores flow less CO_2 and hence less asphaltene is deposited. However, the asphaltene has a greater potential to cause permeability decline because the pathways for fluid flow are smaller and less well connected. Hence, the similarity in K_{db} between all cores near the injection face is simply due to the proportionality between initial permeability and the potential for damage which that permeability provides through asphaltene precipitation.

In the high permeability long core, K_{db} gradually increases along the injection direction, and then drops rapidly after reaching its maximum in the middle of the core (L=17 cm), and finally the value at the outlet end is smaller than at the inlet end. One possible reason for this is that the CO_2 injected at the injection end and the middle part interacts with the crude oil to a greater extent, resulting in a large amount of asphaltene precipitation, which is continuously captured and accumulated during the migration of the fluid, blocking or reducing pores and throats, and which then accelerates the capture of asphaltene precipitation particles. Consequently, the asphaltene precipitation trapped by the pore throats accumulates in a large amount in the middle of the long cores. The amount of asphaltene precipitation along the injection direction becomes progressively less, and the K_{db} value also becomes smaller. The value of K_{db} after the CO_2-SAG process is higher than that after miscible CO_2 flooding. The CO_2 soaking produces more asphaltene precipitation, and the secondary flooding increases the movement of the fluid carrying the asphaltene precipitation, enhancing the filtration of the asphaltene precipitation in the fluid by the pore throats. The value of K_{db} in the low and medium permeability long cores decreases continuously along the injection direction, and the K_{db} value of the low permeability layer decreases rapidly. this is also due to the position of the displacement front that determines the distribution of K_{db}.

688

689 The K_{db} values at the middle of the three long cores are quite different, while the K_{db} values of
690 the middle and low permeability long cores at the outlet end are similar, but are different from
691 those values for the high permeability long core. The distribution of K_{db} at the middle and outlet
692 is similar to that of K_d. This is also due to the position of the CO_2 flooding front in the medium
693 and low permeability layers. It also shows that blockage is the dominant factor in determining
694 K_d in the middle of the long cores and at their outlets.

695

696 In addition, there is a certain difference in K_{db} at the inlet end of the low and medium
697 permeability layers after CO_2-SAG and miscible CO_2 flooding, indicating that CO_2 soaking and
698 secondary flooding increase the degree of asphaltene precipitation to block pores. At the outlet
699 end, CO_2 soaking and secondary displacement have little effect on the degree of asphaltene
700 precipitation to block pore throats.

701

702 After CO_2 flooding, the R_b values at the injection end of the three long cores are similar, the
703 difference between them becoming larger along the core in the direction of flooding (Figure
704 14). The R_b of the core at L=0-27 cm in the high permeability long core remains almost
705 unchanged, and the R_b value of the cores decreases slowly at L =27-50 cm. However, R_b in the
706 low and medium permeability long cores gradually decreases along the injection direction.

707

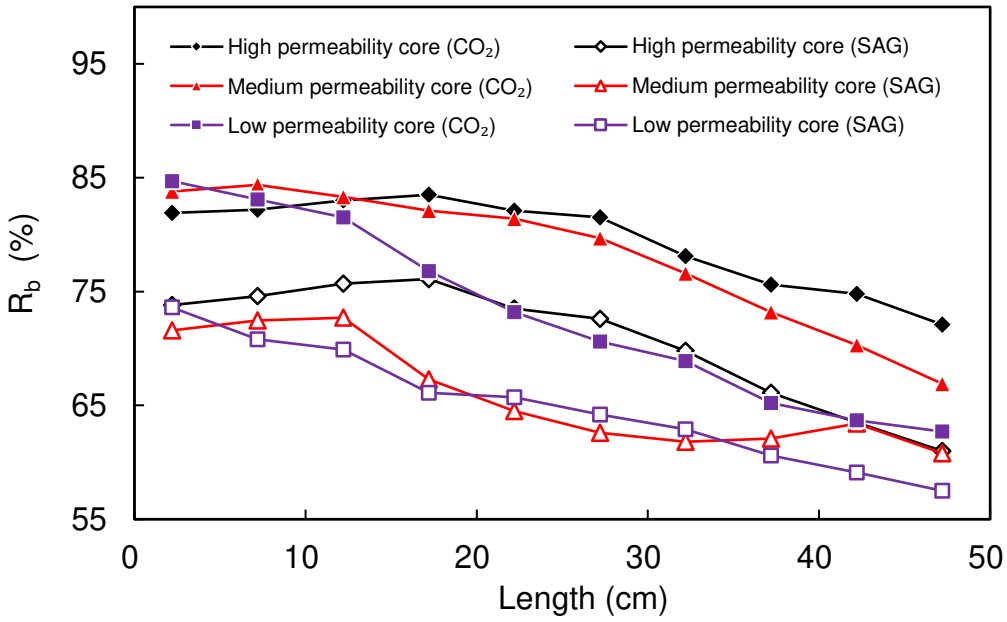

708

709 **Figure 14.** The distribution along cores after flooding of the amount of permeability
710 reduction attributed to pore throat blocking with respect to the total permeability reduction
711 and expressed as a percentage, R_b.

712

713 Although CO_2 BT occurred in the high permeability layer, the flooding front advanced to the
714 outlet end. However, compared with the cores at the injection end and the middle, the
715 interaction between crude oil and CO_2 at the outlet end is not so strong, and the pores swept by
716 CO_2 are also fewer. In the low and medium permeability long cores, the locations near the outlet
717 end are not even swept by CO_2. It seems that the sweeping and flooding of CO_2 is the key factor
718 for pore throat blockage by asphaltene precipitation. It is possible that the complex two phase
719 flow of oil and gas is more likely to cause pore throat blockage instead of causing the adsorption
720 of asphaltene. The two phase flow of gas and oil near the outlet end is less than at the injection
721 end, hence the influence of asphaltene adsorption on the permeability damage gradually
722 increases towards the outlet end of the core[44].

723

The R_b value exhibited by the high permeability long core is the largest of all three. This is because (i) the injected CO_2 flows predominantly through this core, (ii) the flow rate in this core is largest, (iii) the two phase flow of oil and gas is more complex, and (iv) asphaltene precipitation blockage in this core leads to a higher percentage of permeability decline. In addition, the R_b value after SAG flooding is lower than that of CO_2 flooding. This is due to the fact that no fluid migration occurs during the soaking stage, and the asphaltenes produced during the soaking stage reduce the permeability in an adsorbed state.

After SAG flooding, the R_b values of the three layers at the injection end are relatively close, and the R_b value of the high permeability layer is the largest. The distributions of R_b in the low and medium permeability long cores are relatively close, and the difference between the high and medium permeability long cores in the middle of long cores is larger. After CO_2 flooding and SAG flooding, the R_b distribution trend of the medium permeability layer is quite different, which indicates that the CO_2 soaking in the middle of the medium permeability long core has a greater influence on the adhesion state of asphaltene particles, which leads to an increase in the proportion of adsorbed asphaltene. It is worth noting that $K_{db}(SAG) > K_{db}(CO_2)$, however $R_b(SAG) < R_b(CO_2)$

Regardless of the displacement method, the damage to rock permeability (>55%) caused by asphaltene precipitation blockage in pore throats is higher than the damage caused by asphaltene adsorption. This is because pore blockage damages the connectivity between the pores and pore throats in a targeted manner. By contrast, asphaltene adsorption only reduces the size of both pores and pore throats wherever the precipitation occurs. While rock permeability will occur by such a mechanism most of the adsorption has no effect on overall pore connectivity and that which happens to occur at the site of pore throats closes them only slowly and often partially, thus retaining much of the previous connectivity[45].

During the process of recovering the core permeability by cleaning the core of asphaltene deposits and hence removing pore throat blockages and adsorbed asphaltene precipitation, which occurred after flooding, it was observed that the asphaltene blocking pore throats was easier to remove than the adsorbed asphaltene precipitation, the latter of which required a large volume of solvents for long-term cycle cleaning. It is worth noting that the permeability values of all core plunger were tested again after being thoroughly cleaned, the permeability of the same long core at different positions fluctuates less than 3%, and the homogeneity of the long cores is confirmed.

The values of ΔK_{da} (ΔK_{da} (%) = K_{da}(SAG)- K_{da}(CO_2)) are the difference in permeability (K_{da}) of the layers with the same permeability caused by asphaltene adsorption after the two types of flooding process. The distributions of ΔK_{da} along each of the three long cores are shown in Figure 15. The ΔK_{da} in the high permeability long core gradually increases along the injection direction, which indicates that compared with CO_2 flooding, the closer to the outlet end, the stronger the tendency of asphaltene precipitation absorption caused by CO_2 soaking. This is due to there being more residual oil with higher asphaltene content in the cores near the outlet end at the beginning of the CO_2 soaking process.

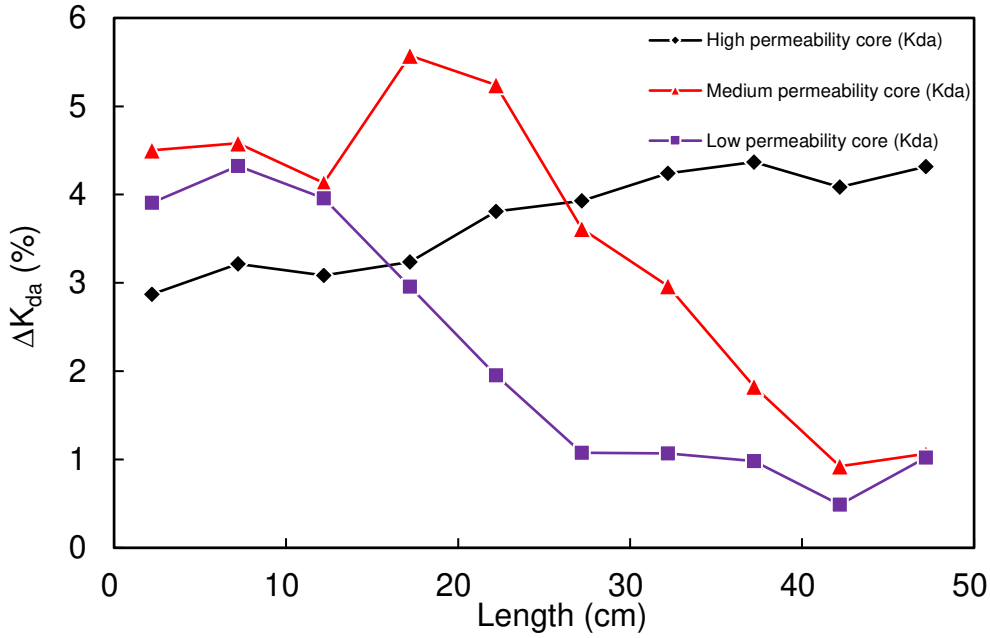

Figure 15. The distribution of the difference in the permeability damage caused by asphaltene adsorption, ΔK_{da} between the two flooding processes.

However, the distribution trends of ΔK_{da} in the low and medium permeability cores are just the opposite, showing a downward trend along the injection direction. This pattern is also partially the effect of the CO_2 flooding front stays in the cores after CO_2 BT in the high permeability long core, which causes CO_2 soaking to increase asphaltene precipitation adsorption at the injection end and also towards the middle of the medium and low permeability long core. This is also confirmed by the fact that the ΔK_{da} of the high-permeability layer at the injection end is much larger than that of the low and medium permeability long core.

Conclusions

Reservoir condition miscible CO_2 flooding and CO_2-SAG flooding experiments have been carried out on 'multilayer' sandstone system. The distributions of differential pressure, residual oil, recovery factor and permeability damage by asphaltene precipitation blockage and adsorption were quantified. The main findings are summarized below.

The overall oil recovery factors after CO_2-SAG flooding for the high, medium and low permeability long cores, are 7.6%, 8.3%, 7.7% higher than conventional CO_2 flooding. The fractional oil production of the high, medium and low permeability long cores were 61.6%, 27.7%, 10.6% after CO_2-SAG flooding, the difference between each layer is less than for conventional CO_2 flooding.

The displacement fronts in the low and medium permeability layers are not significantly advanced due to the soaking stage, which does not significantly expand the sweeping volume, and only enhances the CO_2 displacement effect in the pores that have been swept by CO_2 before CO_2 BT.

After conventional CO_2 flooding, the permeability of the high permeability core near the injection end has a relatively homogeneous drop distribution by 24.5-25.8%, which is 5.5-14.3% higher than that of the core near the outlet end, and gradually decreases. The reduction in permeability for CO_2-SAG flooding is larger than that for conventional CO_2 flooding.

The percentage permeability drop caused by asphaltene precipitation blockage is 84.7-62.7% of the total permeability drop after CO_2 flooding, which represents 5-10% greater decrease in permeability than that caused by CO_2-SAG flooding.

Acknowledgments

Thanks are given to the China Scholarship Council for funding the opportunity of the lead author to research at The University of Leeds, UK. This research is supported by National Natural Science Foundation of China, “The formation mechanism of residual gas and liquid in coal seam and the geological constraints for effective production” (41872171).

References

(1) Cao, M. and Gu, Y., 2013. Oil recovery mechanisms and asphaltene precipitation phenomenon in immiscible and miscible CO_2 flooding processes. *Fuel*, 109, pp.157-166.
(2) Lei, H., Yang, S., Zu, L., Wang, Z. and Li, Y., 2016. Oil recovery performance and CO_2 storage potential of CO_2 water-alternating-gas injection after continuous CO_2 injection in a multilayer formation. *Energy & Fuels*, *30*(11), pp.8922-8931.
(3) You, J., Ampomah, W. and Sun, Q., 2020. Development and application of a machine learning based multi-objective optimization workflow for CO_2-EOR projects. *Fuel*, 264, p.116758.
(4) Wang, L., He, Y., Wang, Q., Liu, M. and Jin, X., 2020. Multiphase flow characteristics and EOR mechanism of immiscible CO_2 water-alternating-gas injection after continuous CO_2 injection: A micro-scale visual investigation. *Fuel*, *282*, p.118689.
(5) Qian, K., Yang, S., Dou, H., Wang, Q., Wang, L. and Huang, Y., 2018. Experimental investigation on microscopic residual oil distribution during CO_2 Huff-and-Puff process in tight oil reservoirs. *Energies*, *11*(10), p. 2843.
(6) Wang, Q., Yang, S., Lorinczi, P., Glover, P.W. and Lei, H., 2019. Experimental Investigation of Oil Recovery Performance and Permeability Damage in Multilayer Reservoirs after CO_2 and Water–Alternating-CO_2 (CO_2–WAG) Flooding at Miscible Pressures. *Energy & Fuels*, 34(1), 624-636.
(7) Han, J., Lee, M., Lee, W., Lee, Y. and Sung, W., 2016.Effect of gravity segregation on CO_2 sequestration and oil production during CO_2 flooding. *Applied energy*, 161, 85-91.
(8) Chen, X., Li,Y.,Tang,X.,Huang,Q., Sun,X.,Luo,J., 2021. Effect of gravity segregation on CO_2 flooding under various pressure conditions: Application to CO_2 sequestration and oil production. *Energy*, 2021,226, p.120294.
(9) Khan, M.Y. and Mandal, A., 2021. Improvement of Buckley-Leverett equation and its solution for gas displacement with viscous fingering and gravity effects at constant pressure for inclined stratified heterogeneous reservoir. *Fuel*, 285, p.119172.
(10) Wang, Q., Shen, J., Lorinczi, P., Glover, P., Yang, S. and Chen, H., 2021. Oil production performance and reservoir damage distribution of miscible CO_2 soaking-alternating-gas (CO_2-SAG) flooding in low permeability heterogeneous sandstone reservoirs. *Journal of Petroleum Science and Engineering*, 204, p.108741.
(11) Zhang, J., Zhang, H.X., Ma, L.Y., Liu, Y. and Zhang, L., 2020. Performance evaluation and mechanism with different CO_2 flooding modes in tight oil reservoir with fractures. *Journal of Petroleum Science and Engineering*, p.106950.
(12) Li, Z. and Gu, Y., 2014. Soaking effect on miscible CO_2 flooding in a tight sandstone formation. *Fuel*, 134, pp. 659-668.
(13) Wang, Q., Wang, L., Glover, P. and Lorinczi, P., 2020. Effect of pore-throat microstructure on miscible CO_2 soaking-alternating-gas (CO_2-SAG) flooding of tight sandstone reservoirs. *Energy & Fuels*, 34(8), pp.9450-9462
(14) Jafari, B., Ghotbi, C., Taghikhani, V. and Shahrabadi, A., 2012. Investigation on asphaltene deposition mechanisms during CO_2 flooding processes in porous media: a novel experimental study and a modified model based on multilayer theory for asphaltene adsorption. *Energy & fuels*, 2012,*26*(8), pp.5080-5091.

(15) Lei, H., Yang, S., Qian, K., Chen, Y., Li, Y. and Ma, Q., 2015. Experimental investigation and application of the asphaltene precipitation envelope. *Energy & Fuels*, 29(11), 6920-6927.
(16) Cho, J., Kim, T.H., Chang, N. and Lee, K.S. Effects of asphaltene deposition-derived formation damage on three-phase hysteretic models for prediction of coupled CO_2 enhanced oil recovery and storage performance. *Journal of Petroleum Science and Engineering*, 2019, 172, 988-997.
(17) Wang, Q., Yang, S., Glover, P.W., Lorinczi, P., Qian, K. and Wang, L., 2020. Effect of Pore-Throat Microstructures on Formation Damage during Miscible CO_2 Flooding of Tight Sandstone Reservoirs. *Energy & Fuels*, 34(4), 4338-4352.
(18) Cui, G., Zhu, L., Zhou, Q., Ren, S. and Wang, J., 2021. Geochemical reactions and their effect on CO_2 storage efficiency during the whole process of CO_2 EOR and subsequent storage. *International Journal of Greenhouse Gas Control*, 108, p.103335.
(19) Hematfar, V., Maini, B. and Chen, Z.J., 2018. Experimental investigation of asphaltene adsorption in porous media due to solvent injection and effects on relative permeability. *International Journal of Multiphase Flow*, 99, pp.174-185.
(20) Shen, Z. and Sheng, J., 2017. Investigation of asphaltene deposition mechanisms during CO_2 huff-n-puff injection in Eagle Ford shale. *Petroleum Science and Technology*, 35(20), pp.1960-1966.(21) Li, Z., 2014. Optimum Timing for CO_2-EOR After Waterflooding and Soaking Effect on Miscible CO_2 Flooding in a Tight Sandstone Formation (Doctoral dissertation, Faculty of Graduate Studies and Research, University of Regina).
(22) Norouzi, H., Rostami, B., Khosravi, M., & Shokri Afra, M. J.,2019. Analysis of secondary and tertiary high-pressure gas injection at different miscibility conditions: mechanistic study. *SPE reservoir evaluation & engineering*, *22*(01), 150-160.
(23) Mathur, A., Ali, S., Woodland, C., Hudson, K., Barnes, C., Von Gonten, W.D. and Belanger, C., 2021, July. Using NMR and Steady State Permeability Measurements to Study Drilling Fluid Invasion Into the Tight Mississippian Ratcliffe Carbonate and Its Impact on Oil Production. *In SPE/AAPG/SEG Unconventional Resources Technology Conference. OnePetro*.
(24) Liu, G., Jiang, H., Li, J., Wang, M., Chen, F., Ding, S. and Lu, X., 2015. Evaluation of the performance of polymer gels mixed with asphalt particle as a novel composite profile control system. *Journal of Industrial and Engineering Chemistry*, 26, pp.309-314.
(25) Abedini, A., Farshid, T. On the CO_2 storage potential of cyclic CO_2 injection process for enhanced oil recovery. *Fuel*, 2014, 124, 14-27.
(26) Abedini, A., Torabi, F. Oil recovery performance of immiscible and miscible CO_2 huff-and-puff processes. *Energy & Fuels*, 2014, 28(2), 774-784.
(27) Li, S., Qiao, C., Li, Z. and Hui, Y., 2018. The effect of permeability on supercritical CO_2 diffusion coefficient and determination of diffusive tortuosity of porous media under reservoir conditions. *Journal of CO_2 Utilization*, 28, pp.1-14.
(28) Jin F., Chen S., Wei B., Wang, D., Yang, W., Wang, Y., Lu, J., 2021.Visualization of CO_2 foam generation, propagation and sweep in a complex 2D heterogeneous fracture network. *Fuel*, 302: 121000.

(29) Cui, G., Wang, Y., Rui, Z., Chen, B., Ren, S. and Zhang, L., 2018. Assessing the combined influence of fluid-rock interactions on reservoir properties and injectivity during CO_2 storage in saline aquifers. *Energy*, 155, pp.281-296.
(30) Nowrouzi, I., Manshad, A.K. and Mohammadi, A.H., 2019. Effects of dissolved carbon dioxide and ions in water on the dynamic interfacial tension of water and oil in the process of carbonated smart water injection into oil reservoirs. *Fuel*, 243, pp.569-578.
(31) Yang, D., Gu, Y. and Tontiwachwuthikul, P., 2008. Wettability determination of the reservoir brine-reservoir rock system with dissolution of CO_2 at high pressures and elevated temperatures. *Energy & Fuels*, *22*(1), pp.504-509.
(32) Al-Bayati, D., Saeedi, A., Myers, M., White, C. and Xie, Q., 2019. An Experimental Investigation of Immiscible- CO_2 -Flooding Efficiency in Sandstone Reservoirs: Influence of Permeability Heterogeneity. *SPE Reservoir Evaluation & Engineering*, 22(03), pp.990-997.
(33) Cui, M., Wang, R., Lv, C. and Tang, Y., 2017. Research on microscopic oil displacement mechanism of CO_2 EOR in extra-high water cut reservoirs. *Journal of Petroleum Science and Engineering*, 154, pp.315-321.
(34) Li, S., Wang, Q., Zhang, K. and Li, Z., 2020. Monitoring of CO_2 and CO_2 oil-based foam flooding processes in fractured low-permeability cores using nuclear magnetic resonance (NMR). *Fuel*, 263, p.116648.
(35) Fassihi, R., Turek, E., Honarpour, M. and Fyfe, R., 2020, August. Investigation of Permeability Impairment Due to Asphaltene Precipitation During Gas Injection EOR in a Major GoM Field. *In SPE Improved Oil Recovery Conference*. OnePetro.
(36) Zanganeh, P., Dashti, H. and Ayatollahi, S., 2018. Comparing the effects of CH_4, CO_2, and N_2 injection on asphaltene precipitation and deposition at reservoir condition: A visual and modeling study. *Fuel*, 217, pp.633-641.
(37) Abouie, A., Tagavifar, M. and Sepehrnoori, K., 2018, April. Wettability alteration and flow coupling in gas flooding of asphaltenic reservoirs. *In SPE Improved Oil Recovery Conference*. OnePetro.
(38) Glover, P.W.J. and Walker, E., 2008. Grain-size to effective pore-size transformation derived from electrokinetic theory. *Geophysics*, 74(1), pp. E17-E29.
(39) Fakher, S. and Imqam, A., 2019. Asphaltene precipitation and deposition during CO_2 injection in nano shale pore structure and its impact on oil recovery. Fuel, 237, pp.1029-1039.
(40) Kord, S., Mohammadzadeh, O., Miri, R. and Soulgani, B.S., 2014. Further investigation into the mechanisms of asphaltene deposition and permeability impairment in porous media using a modified analytical model. Fuel, 117, pp.259-268.
(41) Sim, S.S.K., Okatsu, K., Takabayashi, K. and Fisher, D.B., 2005, October. Asphaltene-induced formation damage: effect of asphaltene particle size and core permeability. *In SPE Annual Technical Conference and Exhibition. OnePetro.*
(42) Minssieux, L., 1997, February. Core damage from crude asphaltene deposition. *In International Symposium on Oilfield Chemistry. OnePetro*.
(43) Soulgani, B.S., Tohidi, B., Jamialahmadi, M. and Rashtchian, D., 2011. Modeling formation damage due to asphaltene deposition in the porous media. *Energy & Fuels*, 25(2), pp.753-761.

938 (44) Nasri, Z. and Dabir, B., 2014. Network modeling of asphaltene deposition during two-
939 phase flow in carbonate. *Journal of Petroleum Science and Engineering*, 116, pp.124-135.
940 (45) Davudov, D. and Moghanloo, R.G., 2019. A new model for permeability impairment due
941 to asphaltene deposition. *Fuel*, 235, pp.239-248.